BBA - General Subjects 1864 (2020) 129433

Contents lists available at ScienceDirect

BBA - General Subjects

journal homepage: www.elsevier.com/locate/bbagen

Flow stimulates drug transport in a human kidney proximal tubule-on-a-chip independent of primary cilia

Jelle Vriend[a,*], Janny G.P. Peters[a], Tom T.G. Nieskens[a], Renata Škovroňová[a], Nina Blaimschein[a], Miriam Schmidts[b,c], Ronald Roepman[b], Tom J.J. Schirris[a,d], Frans G.M. Russel[a,d], Rosalinde Masereeuw[e], Martijn J. Wilmer[a]

[a] Department of Pharmacology and Toxicology, Radboud Institute for Molecular Life Sciences, Radboud University Medical Center, Nijmegen, The Netherlands
[b] Department of Human Genetics, Radboud Institute for Molecular Life Sciences, Radboud University Medical Center, Nijmegen, The Netherlands
[c] Center for Pediatrics and Adolescent Medicine, University Hospital Freiburg, Freiburg University Faculty of Medicine, Freiburg, Germany
[d] Centre for Systems Biology and Bioenergetics, Radboud Center for Mitochondrial Medicine, Radboud University Medical Center, The Netherlands
[e] Division of Pharmacology, Utrecht Institute for Pharmaceutical Sciences, Utrecht, The Netherlands

ARTICLE INFO

Keywords:
Flow
PTEC
Proximal tubule-on-a-chip
Primary cilia
Drug transport
Nephrotoxicity

ABSTRACT

Background: Kidney disease modeling and assessment of drug-induced kidney injury can be advanced using three-dimensional (3D) microfluidic models that recapitulate *in vivo* characteristics. Fluid shear stress (FSS) has been depicted as main modulator improving *in vitro* physiology in proximal tubule epithelial cells (PTECs). We aimed to elucidate the role of FSS and primary cilia on transport activity and morphology in PTECs.
Methods: Human conditionally immortalized PTEC (ciPTEC-parent) was cultured in a microfluidic 3D device, the OrganoPlate, under a physiological peak FSS of 2.0 dyne/cm^2 or low peak FSS of 0.5 dyne/cm^2. Upon a 9-day exposure to FSS, albumin-FITC uptake, activity of P-glycoprotein (P-gp) and multidrug resistance-associated proteins 2/4 (MRP2/4), cytotoxicity and cell morphology were determined.
Results: A primary cilium knock-out cell model, ciPTEC-KIF3α$^{-/-}$, was successfully established *via* CRISPR-Cas9 genome editing. Under physiological peak FSS, albumin-FITC uptake (p = .04) and P-gp efflux (p = .002) were increased as compared to low FSS. Remarkably, a higher albumin-FITC uptake (p = .03) and similar trends in activity of P-gp and MRP2/4 were observed in ciPTEC-KIF3α$^{-/-}$. FSS induced cell elongation corresponding with the direction of flow in both cell models, but had no effect on cyclosporine A-induced cytotoxicity.
Conclusions: FSS increased albumin uptake, P-gp efflux and cell elongation, but this was not attributed to a mechanosensitive mechanism related to primary cilia in PTECs, but likely to microvilli present at the apical membrane.
General significance: FSS-induced improvements in biological characteristics and activity in PTECs was not mediated through a primary cilium-related mechanism.

1. Introduction

Recent advances in kidney-on-a-chip or renal microfluidic device technology have demonstrated great potential for kidney disease modeling and assessment of drug-induced kidney injury (DIKI) by recapitulating the *in vivo* tissue characteristics. Three-dimensional (3D) kidney models, ranging from microfluidic devices to bioprinted proximal tubules allowed, culturing of renal cells under flow and in combination with an extracellular matrix (ECM), advancing *in vitro* modeling [1–5]. Such models have also gained interest for implementation in pre-clinical drug safety assessment to improve DIKI prediction at early stages of drug development.

Although DIKI has been described for all parts of the nephron [6], drugs mainly affect the proximal tubule epithelial cells (PTECs) as many xenobiotics are actively secreted by membrane transporters present in the cells of this segment, which increases the exposure of cells [7]. This active secretion of xenobiotics is mediated by transport proteins expressed at the basolateral membrane facing the blood vessels or at the apical membrane facing the lumen, and are categorized as members of the ATP-binding cassette (ABC) or solute carrier (SLC) transporter

* Corresponding author at: Department of Pharmacology and Toxicology (137), Radboud Institute for Molecular Life Sciences, Radboud University Medical Center, P.O. Box 9101, 6500 HB Nijmegen, The Netherlands.
E-mail address: jelle.vriend@radboudumc.nl (J. Vriend).

https://doi.org/10.1016/j.bbagen.2019.129433
Received 29 April 2019; Received in revised form 31 July 2019; Accepted 6 August 2019
Available online 11 September 2019
0304-4165/ © 2019 The Author(s). Published by Elsevier B.V. This is an open access article under the CC BY-NC-ND license (http://creativecommons.org/licenses/BY-NC-ND/4.0/).

families. Uptake of organic anions is mediated *via* organic anion transporter 1 and 3 (OAT1, *SLC22A6*; OAT3, *SLC22A8*), expressed at the basolateral membrane, and their efflux is facilitated *via* multidrug resistance-associated proteins 2 and 4 (MRP2, *ABCC2*; MRP4, *ABCC4*) and breast cancer resistance protein (BCRP, *ABCG2*) at the apical membrane. Uptake of organic cations is mediated by basolateral uptake *via* organic cation transporter 2 (OCT2; *SLC22A2*) and apical efflux mainly *via* multidrug and toxin extrusion proteins 1 and 2-k (MATE1, *SLC47A1*; MATE2-k, *SLC47A2*), while efflux of larger cations is mediated by P-glycoprotein (P-gp, *ABCB1*). Upon glomerular filtration, reuptake of proteins, such as albumin, takes places in PTECs through receptor-mediated endocytosis involving megalin (*LRP*) and cubilin (*CBN*), which are expressed at the apical membrane [8]. Most renal drug transporter studies have been performed in conventional two-dimensional static cell cultures, although recently this has also been addressed in 3D kidney models [1,2,9,10].

Fluid shear stress (FSS) was shown to be important for improving *in vitro* biological activity and cell morphology in 3D kidney models [1–3]. PTECs are apically exposed to a pulsatile flow, generated by the pumping action of the heart and the intrarenal hemodynamic control leading to glomerular filtration, which results in FSS [11]. This affects the organization of the cytoskeleton of renal cells, as demonstrated *in vitro* and *in vivo* [12–14]. In addition, it was demonstrated that FSS stimulated polarization of PTECs and their transformation into a columnar-shaped morphology as found *in vivo* [1–3]. Exposing PTECs to FSS resulted in increased albumin uptake and P-gp activity [1,2,15,16], as well as increased transcellular transport of organic cations mediated *via* a concerted action of OCT2 and MATE1 [17].

This shift towards a more *in vivo*-like morphology in PTECs has been attributed to FSS, which is sensed by microvilli, glycocalyx and the primary cilium present at the apical membrane [18]. Primary cilia increased in number in primary collecting duct cells and kidney organoids when cultured under flow [2,19]. Interestingly, enhanced albumin uptake and organic cation transport was not observed in transient chemically-deciliated cells that were exposed to flow [15,17].

In this study, we used human conditionally immortalized PTEC (ciPTEC) in a microfluidic device, the OrganoPlate, to study the long-term effects of exposure to different strengths of pulsatile FSS. Furthermore, we established a stable primary cilium knock-out cell line *via* CRISPR-Cas9 genome editing to deplete KIF3α, a subunit of the primary cilium motor complex kinesin-II, which is required for the assembly of the primary cilium [20]. We aimed to elucidate the role of FSS on drug transport activity, albumin uptake and epithelial cell morphology in ciPTEC-parent in comparison to the primary cilium knock-out ciPTEC line in the OrganoPlate. The aim of this study was to evaluate the role of FSS on tubular transport, albumin uptake and cell morphology in ciPTEC, and whether this was mediated through primary cilium-mediated signaling.

2. Materials and methods

2.1. Cell culture

CiPTEC-parent were obtained as previously described [21]. Proliferating cells were sub-cultured using 1:2 to 1:6 dilutions at 33 °C and 5% (*v/v*) CO_2 in T75 cell culture flasks (Greiner Bio-One, Alphen aan den Rijn, The Netherlands). Medium was refreshed every 2–3 days and consisted of a 1:1 mixture of Dulbecco's modified Eagle's medium and Nutrient mixture F-12 without phenol red (DMEM/F-12, Life Technologies, Paisly, UK), supplemented with insulin (5 μg/mL, Sigma-Aldrich, Zwijndrecht, The Netherlands), transferrin (5 μg/mL, Sigma-Aldrich), selenium (5 ng/mL, Sigma-Aldrich), hydrocortisone (36 ng/mL, Sigma-Aldrich), epidermal growth factor (10 ng/mL, Sigma-Aldrich) trio-iodothyrine (40 pg/mL, Sigma-Aldrich), 1% (v/v) penicillin/streptomycin (Life Technologies) and 10% (v/v) fetal calf serum (FCS, Greiner Bio-One) further referred to as PTEC complete medium. Cells were used for experiments from passage numbers 34 to 58.

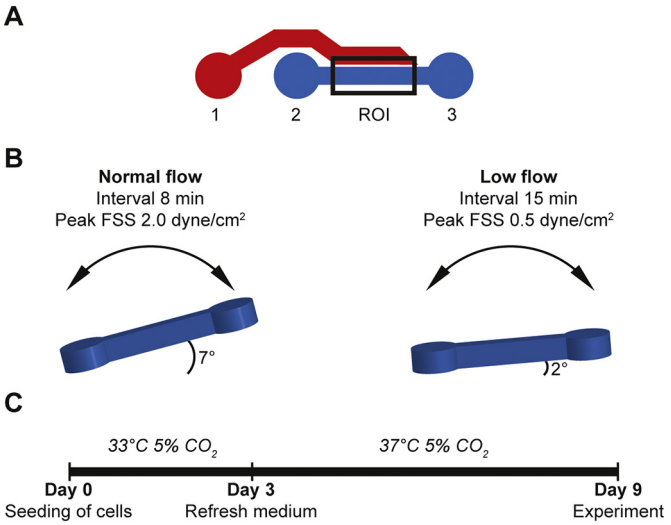

Fig. 1. Schematic presentation of a two-lane chip in the OrganoPlate and experimental set-up, (A) consisting of a gel channel (red) and a perfusion channel (blue). The gel channel is accessible through the gel channel inlet (1) and the perfusion channel is accessible through the medium channel inlet (2) or outlet (3). Cells cultured in the perfusion channel at the extracellular (ECM)-medium interface, indicated by the black box, were exposed to full fluid shear stress (FSS) and set as the region of interest (ROI) in our experiments. (B) FSS was induced by a bi-directional pulsatile flow generated by leveling, of which the peak FSS was influenced by the angle of the platform and the interval of change of position. Settings at normal flow resemble physiological FSS experienced by cells *in vivo*, while settings for low flow were chosen only to have minimal flow for waste removal and supply of nutrients and oxygen. (C) Cells were cultured under FSS at 33 °C for 3 days to allow cell proliferation followed cell maturation at 37 °C for 6 days. (For interpretation of the references to color in this figure legend, the reader is referred to the web version of this article.)

To culture cells in a 3D environment under FSS, ciPTEC-parent was cultured in a microfluidic platform, the two-lane OrganoPlate® (Mimetas, Leiden, The Netherlands). A two-lane OrganoPlate consists of 96 chips, which are divided in a gel channel and a perfusion channel (Fig. 1A). Per chip, an ECM of collagen I (4 mg/mL, Cultrex 3D Collagen I Rat Rail, R&D Systems, Minneapolis, MN, USA) was injected and upon polymerization, 40,000 cells in a suspension of 2 μL were pipetted in the medium channel outlet, as described before [9]. For background correction, chips containing no cells were used by adding 2 μL of PTEC complete medium per chip. Upon seeding, 50 μL of PTEC complete medium was added to the medium channel outlet. The OrganoPlate was placed vertically to allow cells to attach to the ECM at 33 °C and 5% (v/v) CO_2 for 5 h. Then, 50 μL of PTEC complete medium was added to the medium channel outlet. Perfusion was started by placing the OrganoPlate at 33 °C and 5% (*v/v*) CO_2 on a perfusion rocker mini (Mimetas) to generate a pulsatile bi-directional flow induced by leveling (Fig. 1B). Normal flow was induced by leveling at a 7° angle and 8 min interval, corresponding to a pulsatile flow with a peak FSS of 2.0 dyne/cm^2, which is within range of FSS used in other studies on PTECs and estimation of FSS *in vivo* [10,22]. Low flow was induced by leveling at a 2° angle and 15 min interval, corresponding to a peak FSS of 0.5 dyne/cm^2, which is used as minimal flow required for waste removal and supply of nutrients and oxygen.

On day 3 after seeding, medium in chips were refreshed with PTEC complete medium without penicillin/streptomycin, and placed at 37 °C and 5% (*v/v*) CO_2 on a perfusion rocker mini, to allow cell differentiation under the corresponding flow (Fig. 1C). Medium was refreshed every 2–3 days. On day 9 after seeding, experiments were performed while maintaining the corresponding flow on the perfusion rocker during experimental incubations described below (Fig. 1C).

2.2. Knock-out of KIF3α in ciPTEC

A ciPTEC line exhibiting stable knock-out of KIF3α, a component of the primary cilium kinesin-II motor complex, was obtained *via* CRISPR-Cas9 gene-editing. The primers were designed using the human KIF3α target sequence GGTCATATTGCAAAAGCGGAGG, as previously described [23], and obtained from Biolegio (Nijmegen, The Netherlands). The annealed primers were ligated into the pSpCas9(BB)-2A-GFP (PX458) plasmid (gift from Feng Zhang, Addgene 48138) [24]. This resulting plasmid was transformed in Stbl3 competent cells (Invitrogen, Carlsbad, CA, USA). The sequence was confirmed and the yield of the plasmid was increased subsequently. Next, ciPTECs were seeded at 60,000 cells/cm^2 in 6-well plates 24 h prior transfection. CiPTECs were then transfected with 2.5 μg PX458 plasmid, containing the target sequence, per well using Lipofectamin 3000 reagent (Invitrogen) in Opti-MEM I (Invitrogen) serum-free medium at 33 °C and 5% (*v/v*) CO_2. After 48 h, green fluorescent protein-positive cells were sorted on a Becton Dickinson (BD) FACS Aria (BD Bioscience, Breda, The Netherlands) and single cells were plated in 96-well plates. Cells were cultured at 33 °C and 5% (*v/v*) CO_2 to 80–90% confluency. After approximately 3 weeks genomic DNA was extracted using QIAamp DNA mini kit (Qiagen, Venlo, The Netherlands) and the sequence was pre-amplified using PCR (forward primer: GCAAAACTTTTACCATGGAAGG, reverse primer: TCCAAATAAGACACTCGAACCA) at 63 °C for 35 cycles with Q5 high-fidelity polymerase (New England Biolabs, Ipswich, MA, USA). PCR products were treated with ExoSAP-IT (Applied Biosystems, Bleijswijk, The Netherlands) and sequenced using the primers described above. One clone containing the targeted knock-out was obtained, establishing the ciPTEC-KIF3α$^{-/-}$ cell line. CiPTEC-KIF3α$^{-/-}$ cells were cultured in T75 cell culture flasks and in the OrganoPlate as described above for ciPTEC-parent cells.

2.3. Western blotting of KIF3α

Knock-out of KIF3α was measured on protein level using Western blotting in proliferated and matured ciPTEC-parent and ciPTEC-KIF3α$^{-/-}$. Proliferating cells were cultured at 33 °C and 5% (*v/v*) CO_2 to 80–90% confluency, as above described. To obtain a matured cell monolayer, cells were seeded at 55,000 cells/cm^2 in a T75 cell culture flask, cultured at 33 °C and 5% (*v/v*) CO_2 for 1 day, and subsequently cultured at 37 °C and 5% (*v/v*) CO_2 for 7 days to allow cells to differentiate. Cell pellet was harvested, resuspended in cold (4 °C) buffer containing 1% (*v/v*) IGEPAL® CA-630 (Sigma-Aldrich), 0.5% (*w/v*) sodium deoxycholate (Sigma-Aldrich), 0.1% (*w/v*) sodium dodecyl sulfate (SDS, Serva, Heidelberg, Germany), 1 mM phenylmethanesulfonyl fluoride (PMSF, Sigma-Aldrich), 3% (*v/v*) aprotinin from bovine lung (Sigma-Aldrich) and 1 mM sodium orthovanadate (Sigma-Aldrich). Next, 1% (*v/v*) DNase I (Invitrogen) was added and samples were incubated on ice for 30 min. Protein levels were measured using a Bio-Rad protein assay (Bio-Rad, Veenendaal, The Netherlands), according the manufacturer's protocol, and samples were loaded on a 10% (*w/v*) poly-acrylamide SDS-PAGE gel for electrophoresis. Membranes were incubated with primary antibodies against KIF3α (monoclonal, 1:1000, rabbit, Abcam, Cambridge, UK) or β-actin (clone AC-15, 1:10,000, mouse, Sigma-Aldrich), as loading control, at 4 °C overnight, followed by incubation with corresponding secondary antibodies IRDye® 800CW NHS ester goat anti-rabbit (1:10,000, Li-Cor Biosciences, Lincoln, NE, USA) or Alexa Fluor® 680 donkey anti-mouse (1:10,000, Invitrogen) at room temperature for 1 h. Fluorescence was detected using the Odyssey scanner CLx (Li-Cor Biosciences).

2.4. Albumin-FITC uptake

Uptake of albumin-fluorescein isothiocyanate conjugate (albumin-FITC, 50 μg/mL, Sigma-Aldrich) was determined with or without bovine serum albumin (BSA, 10 mg/mL, Roche, Almere, The Netherlands). Albumin-FITC and Hoechst33342 (Life Technologies) were dissolved in Tris-HCl (10 mM, Invitrogen) pH 7.0 and milli-Q water, respectively. Dilutions of albumin-FITC and Hoechst33342 were prepared in PTEC serum-free medium, BSA was dissolved directly in PTEC serum-free medium. Chips were first washed by adding 50 μL PTEC serum-free at 37 °C to medium channel inlet and outlet and subsequently perfused twice. Perfusion in chips during washing was induced by pipetting 20 μL and 80 μL to the medium channel inlet and outlet, respectively. Albumin uptake was performed at 37 °C and 5% (*v/v*) CO_2 for 4 h. Next, cell nuclei were stained with Hoechst33342 (20 μg/mL) in cold (4 °C) PTEC serum-free medium, perfusion was induced by adding 20 μL and 80 μL to the medium channel inlet and outlet, respectively. Albumin-FITC uptake in chips was imaged immediately after staining of cell nuclei.

2.5. 3D fluorescent efflux assays P-gp and MRP2/4

Activities of MRP2/4 and P-gp were determined as described for ciPTEC in 2D and 3D cell culture [9,25]. MRP2/4 activity was measured using 5-chloromethylfluorescein diacetate (CMFDA, 1.25 μM, Life Technologies), which freely diffuses into the cell and is then metabolized into the fluorescent glutathione-methylfluorescein (GS-MF), a substrate for MRP2/4. A combination of PSC833 (5 μM, Tocris, Bristol, UK), MK571 (10 μM, Sigma-Aldrich) and KO143 (10 μM, Sigma-Aldrich) was used to inhibit efflux of CMFDA and GS-MF *via* P-gp, MRP2/4 and BCRP, respectively. Calcein-acetoxymethyl (calcein-AM, 2 μM, Life Technologies) was used to determine P-gp activity with or without the presence of inhibitors PSC883 (5 μM) or cyclosporine A (CsA, 30 μM, Sigma-Aldrich). Calcein-AM, a P-gp substrate, is cell membrane permeable and metabolized into the fluorescent calcein by cellular esterase. Stocks of CMFDA, calcein-AM, PSC833, KO143 and CsA were prepared in DMSO (Sigma-Aldrich). MK571 was dissolved in milli-Q water. All dilutions were prepared in Krebs-Henseleit buffer (Sigma-Aldrich) and HEPES (10 mM, Sigma-Aldrich) at pH 7.4, further referred to as KHH. Cells were exposed to corresponding vehicles, final concentration of DMSO did not exceed 0.3% (*v/v*). Prior to exposure, chips were washed and perfused using KHH at 37 °C as described above. Incubation with CMFDA or calcein-AM with inhibitors or vehicle were then performed at 37 °C and 5% (*v/v*) CO_2 for 1 h. After incubation, chips were perfused and cell nuclei were stained with Hoechst33342 (20 μg/mL) in cold (4 °C) KHH containing PSC833 (5 μM), MK571 (10 μM), KO143 (10 μM), to block any further efflux, directly followed by imaging of intracellular GS-MF and calcein accumulation per chip.

2.6. Gene expression

RNA from chips in the OrganoPlate was extracted as described before [9]. Briefly, RNA from cells cultured in the OrganoPlate were isolated using the RNeasy Micro Kit (Qiagen). Complementary DNA (cDNA) was attained using Moloney Murine Leukemia Virus (M-MLV, Invitrogen) reverse transcriptase, according to the manufacturer's protocol. Gene expression levels of drug transporters *ABCB1* (hs01067802_m1), *ABCC2* (hs00166123_m1), *ABCC4* (hs00195260_m1), *SLC22A2* (hs01010723_m1), *SLC47A1* (hs00217320_m1), *SLC47A2* (hs00945650_m1) and endocytosis receptors *LRP* (hs00189742_m1) and *CBN* (hs00153607_m1) were assessed. In addition, gene expression levels of claudin-2 (*CLDN2*, hs002526665_s1), a component of the tight junction in PTECs; heme oxygenase-1 (HO-1, *HMOX1*, hs01110250_m1), an oxidative stress marker; and hypoxia inducible factor 1 alpha (HIF1α, *HIF1A*, hs00153153_m1), a hypoxia marker, were measured. Expression levels of *GADPH* (hs99999905_m1) and *HPRT1* (Hs02800695_m1) were used as reference genes. Gene specific primer-probe sets and TaqMan Universal PCR Master Mix were purchased from Applied Biosystems. Quantitative PCR (qPCR) reactions were measured using CFX96-Touch Real-Time PCR System (Bio-Rad) and analyzed using Bio-Rad CFX

Manager (version 3.1). Gene expression levels were normalized to expression levels of *GAPDH* and expressed as fold difference compared to average gene expression levels in cells cultured under normal flow from three independent experiments.

2.7. Immunofluorescent staining

For immunofluorescent staining, chips were fixated, washed and blocked as described previously [9]. Briefly, cells were treated with primary antibodies against pericentrin (1:500, rabbit, Abcam), a centrosome marker; acetylated-tubulin (clone 6-11B-1, 1:1000, mouse, Sigma-Aldrich), a component of the primary cilium; and zona occludens-1 (ZO-1, 1:125, rabbit, Life Technologies), a tight junction protein. Next, chips were exposed to corresponding secondary antibodies, using Alexa Fluor® 647 goat anti-rabbit (1:250, Life Technologies), Alexa Fluor® 488 goat anti-mouse (1:250, Life Technologies) and Alexa Fluor® 488 goat anti-rabbit (1:250, Abcam), respectively. Additionally, cell nuclei and F-actin were stained using DAPI (300 nM, Life Technologies) and ActinRed 555 (Life Technologies), according to the manufacturer's protocol, in Hank's balanced salt solution (HBSS, Life Technologies), respectively. Fluorescent images were acquired using a Zeiss LSM880 laser scanning confocal microscope (Carl Zeiss, Jena, Germany). *Z*-stacks of pericentrin and acetylated-tubulin were acquired using a ×40 water immersion objective, over a range of 18 μm with a 1 μm interval. Per image, nuclei and primary cilia were counted, and then expressed as number of primary cilia observed as percentage of total nuclei count. The average length of primary cilia (in μm) was determined for 10 primary cilia per image. For imaging of ZO-1, *Z*-stacks were imaged using ×40 water immersion objective, over a range of 20 μm with a 0.57 μm interval. Reconstructions of PTEC tubules in the OrganoPlate were obtained by imaging F-actin using a ×20 objective over a range of 160 μm with a 2 μm interval. Z-stacks were combined and maximum intensity was displayed in Fiji software (version 1.51n) [26]. For 3D renderings, images were adjusted for windows and level and projected in 3D animations in Fiji.

2.8. Cell viability

Cells were exposed to CsA (30 μM) or corresponding vehicle (0.2% (*v/v*) DMSO) on day 8 after seeding at 37 °C and 5% (*v/v*) CO_2 for 24 h. Stocks of propidium iodide (Sigma-Aldrich) and YO-PRO-1 (Life Technologies) were dissolved in milli-Q water and DMSO, respectively. Next, necrotic cells were stained with propidium iodide (1 μg/mL), apoptotic cells with YO-PRO-1 (2 μM), and cell nuclei with Hoechst33342 (20 μg/mL) in KHH at 37 °C for 20 min. Perfusion in chips was initiated by adding 20 μL and 80 μL to the medium channel inlet and outlet, respectively.

2.9. Intracellular calcium staining

To measure intracellular levels of Ca^{2+} upon culturing under normal flow, cells in chips were stained with Fluo-4, AM (Life Technologies), which was dissolved in DMSO. Before staining, chips perfused once with KHH at 37 °C, as described above. Next, cells were stained with Fluo-4, AM (10 μM) and Hoechst33342 (20 μg/mL) at 37 °C and 5% (*v/v*) CO_2 for 20 min followed by incubation at room temperature for 20 min. For measurement of intracellular levels of Ca^{2+} upon induction of fluid flow *in situ*, 40 μL of medium was transferred from the medium outlet to the medium inlet, followed by direct measurement of fluorescence intensity of Fluo-4. Final concentration of DMSO was 1% (*v/v*) in all conditions.

2.10. Fluorescent live-cell imaging and analysis

For live-cell imaging, a BD Pathway 855 high-throughput microscope (BD Bioscience) with a ×10 objective was used. Fluorescence intensity of albumin-FITC, GS-MF, calcein, Fluo-4 and YO-PRO-1 were acquired using a 488 nm excitation filter and 520 nm emission filter. Hoechst33342 images were acquired with a 360 nm excitation filter and a 460 nm emission filter. Propidium iodide staining was imaged using a 548 nm excitation filter in combination with a 645 nm emission filter.

To quantify accumulation of albumin-FITC, GS-MF and calcein, images were corrected for background intensity, using an image of a chip containing no cells and treated with corresponding probes. Per chip, intensity was determined and cell nuclei count was determined by masking Hoecsht33342 images upon background correction in Fiji. Then, average fluorescence intensity, corrected for cell nuclei count, was normalized to fluorescent/nuclei count ratio in control of normal flow in same experiment.

Cell morphology was assessed using intracellular calcein staining upon background correction as above described. Cell surface area, aspect ratio and circularity were all determined by creating a cell mask of calcein staining in Fiji. Per image, 10 single-cells were selected and cell surface area (in μm^2), aspect ratio (major axis divided by minor axis) and circularity ($(4\pi*\text{area})/\text{perimeter}^2$) were determined.

For cell viability, Hoechst33342, YO-PRO-1 and propidium iodide images were corrected for background and cell nuclei were counted in Hoechst33342 images in Fiji, as described above. A mask of Hoechst33342 images was used to determine YO-PRO-1 and propidium iodide positive cells, corresponding to count of dead cells. Cell viability was then calculated as percentage of live cells compared to total number of cell nuclei.

For each chip, Fluo-4 images were corrected for background by subtracting average intensity from a region of background pixels containing no fluorescent signal. Integrated density per chip was determined and corrected for cell nuclei count in Fiji.

2.11. Statistical analysis

Data are presented as mean ± SEM for 2 to 3 chips per condition from three independent experiments ($n = 3$), unless stated otherwise. Statistics were performed using GraphPad Prism version 8 (San Diego, CA, USA). Means of normal flow were found to be significantly different compared to low flow in the same cell line if $p < .05$, using an unpaired two-sided Student's *t*-test, unless stated otherwise.

Table 1
Gene expression levels of drug transporters, endocytosis receptors, tight junction proteins and oxidative status markers in ciPTEC-parent.

Gene	Ct values		$2^{-\Delta\Delta Ct}$	
	Normal flow	Low flow	Normal flow	Low flow
GAPDH	18.9 ± 0.2	19.0 ± 0.1		
HPRT1	26.2 ± 0.1	26.0 ± 0.1	1.0 ± 0.1	0.8 ± 0.0
ABCB1	27.7 ± 0.3	28.0 ± 0.5	1.0 ± 0.2	0.8 ± 0.2
ABCC2	33.9 ± 0.2	33.8 ± 0.1	1.0 ± 0.1	1.0 ± 0.3
ABBC4	25.2 ± 0.1	25.6 ± 0.1	1.0 ± 0.0	0.7 ± 0.1*
SLC22A2	36.4 ± 0.4	36.7 ± 0.6	1.1 ± 0.3	0.9 ± 0.3
SLC47A1	31.9 ± 1.0	32.4 ± 1.0	1.5 ± 0.9	1.0 ± 0.6
SCL47A2	33.7 ± 1.1	33.2 ± 0.9	1.7 ± 1.2	1.8 ± 1.0
LRP2	38.5 ± 0.6	38.8 ± 0.5	1.2 ± 0.5	0.9 ± 0.3
CBN	32.2 ± 0.4	32.2 ± 0.3	1.0 ± 0.1	0.9 ± 0.1
CLDN2	27.5 ± 0.2	27.2 ± 0.5	1.0 ± 0.1	1.3 ± 0.4
HMOX1	25.4 ± 0.7	25.2 ± 0.2	1.4 ± 0.8	1.1 ± 0.3
HIF1A	20.4 ± 0.1	20.8 ± 0.1	1.0 ± 0.2	0.7 ± 0.2

Levels of mRNA of drug transporters (*ABCB1, ABCC2, ABCC4, SLC22A2, SLC47A1, SLC47A2*), albumin endocytosis receptors (*LRP2, CBN*), a tight junction component (*CLDN2*) and oxidative status markers (*HMOX1, HIF1A*). Student's *t*-test normal flow *vs.* low flow, *$p < .05$.

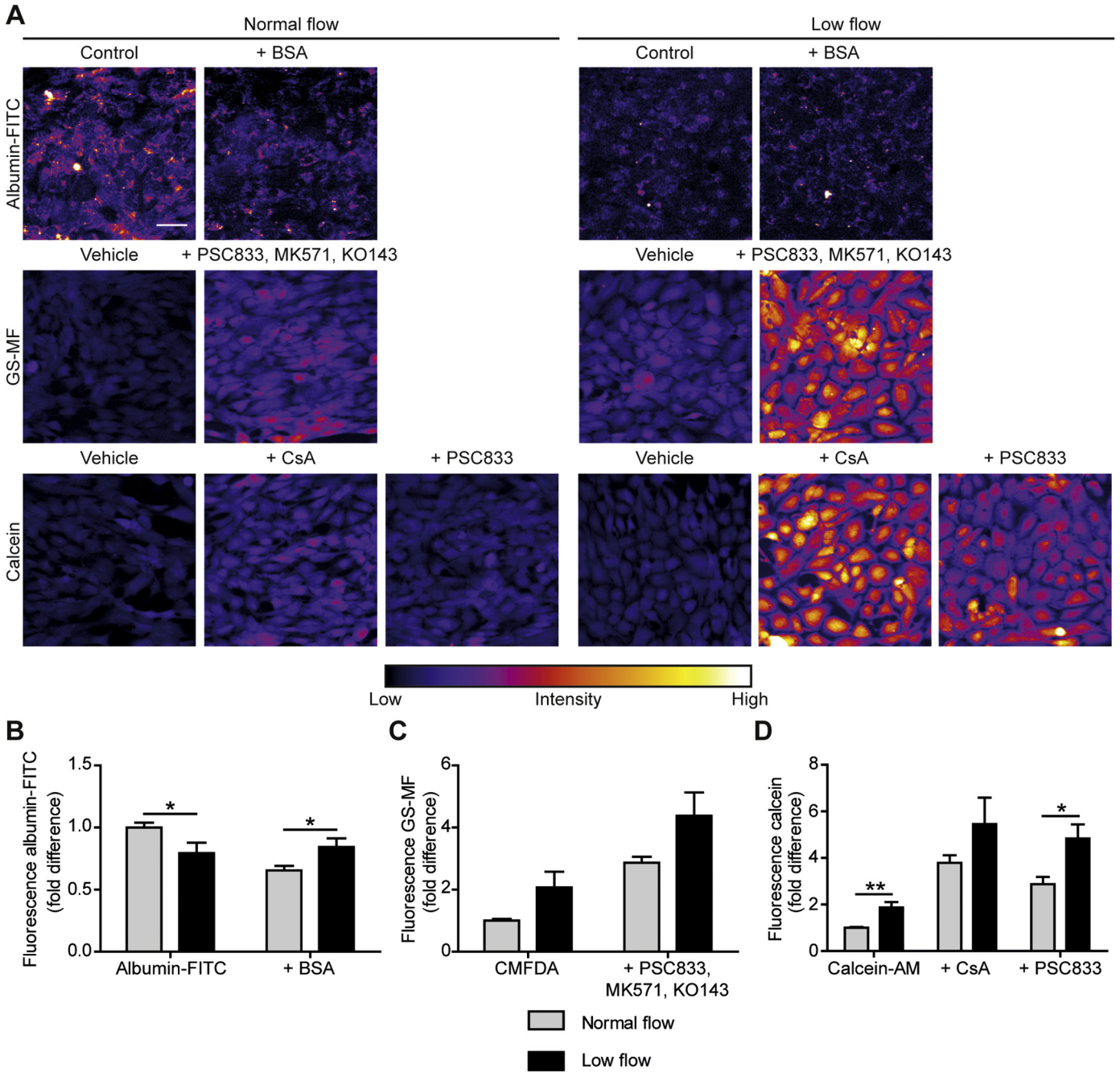

Fig. 2. Albumin uptake and efflux activity of P-glycoprotein (P-gp) and multidrug resistance-associated proteins 2 and 4 (MRP2/4) in ciPTEC-parent cultured under normal and low flow in the OrganoPlate. (A) Representative images of intracellular accumulation of albumin-fluorescein isothiocyanate conjugate (albumin-FITC), glutathione-methylfluorescein (GS-MF) and calcein. Albumin-FITC uptake was visible in all conditions but was decreased upon exposure with bovine serum albumin (BSA, 10 mg/mL) in normal FSS. Accumulation of GS-MF, which corresponds to efflux activity of MRP2/4, was evident in all conditions and increased upon incubation with a mixture of inhibitors PSC833 (5 μM), MK571 (10 μM), KO143 (10 μM). P-gp activity was determined *via* accumulation of calcein. Accumulation was observed in all conditions and increased upon exposure to cyclosporine A (CsA, 30 μM) or PSC833 (5 μM). To enhance contrast for presentation, display ranges of albumin-FITC, GS-MF and calcein images were set to 0 to 600, 0 to 900 and 0 to 1800, respectively. Gray scale values were converted to look-up table (LUT) color fire. Scale bar represents 50 μm, scale in all images are equal. Fluorescent signal was quantified, corrected for nuclei count, using Hoechst33342 (20 μg/mL), and normalized to fluorescence measured in vehicle in normal flow for (B) albumin-FITC, (C) GS-MF and (D) calcein. Student's *t*-test normal flow *vs.* low flow, $*p < .05$, $**p < .01$.

3. Results

3.1. Fluid shear stress-induced increased albumin uptake and P-gp activity

When ciPTECs were cultured in OrganoPlates, clear tubular epithelial monolayers were formed under normal flow conditions, as demonstrated by F-actin staining (Video S1). When exposed to low flow, cells also formed a monolayer on the bottom of the OrganoPlate perfusion channel, which was not formed at the ECM-medium interface (Video S1).

Upon exposure of ciPTEC-parent to normal or low flow, we determined the gene expression levels (Table 1) of relevant drug transporters (*ABCB1*, *ABCC2*, *SLC22A2*, *SLC47A1*, *SLC47A2*), and receptors megalin (*LRP2*) and cubilin (*CBN*). Expression of *ABCC4* was

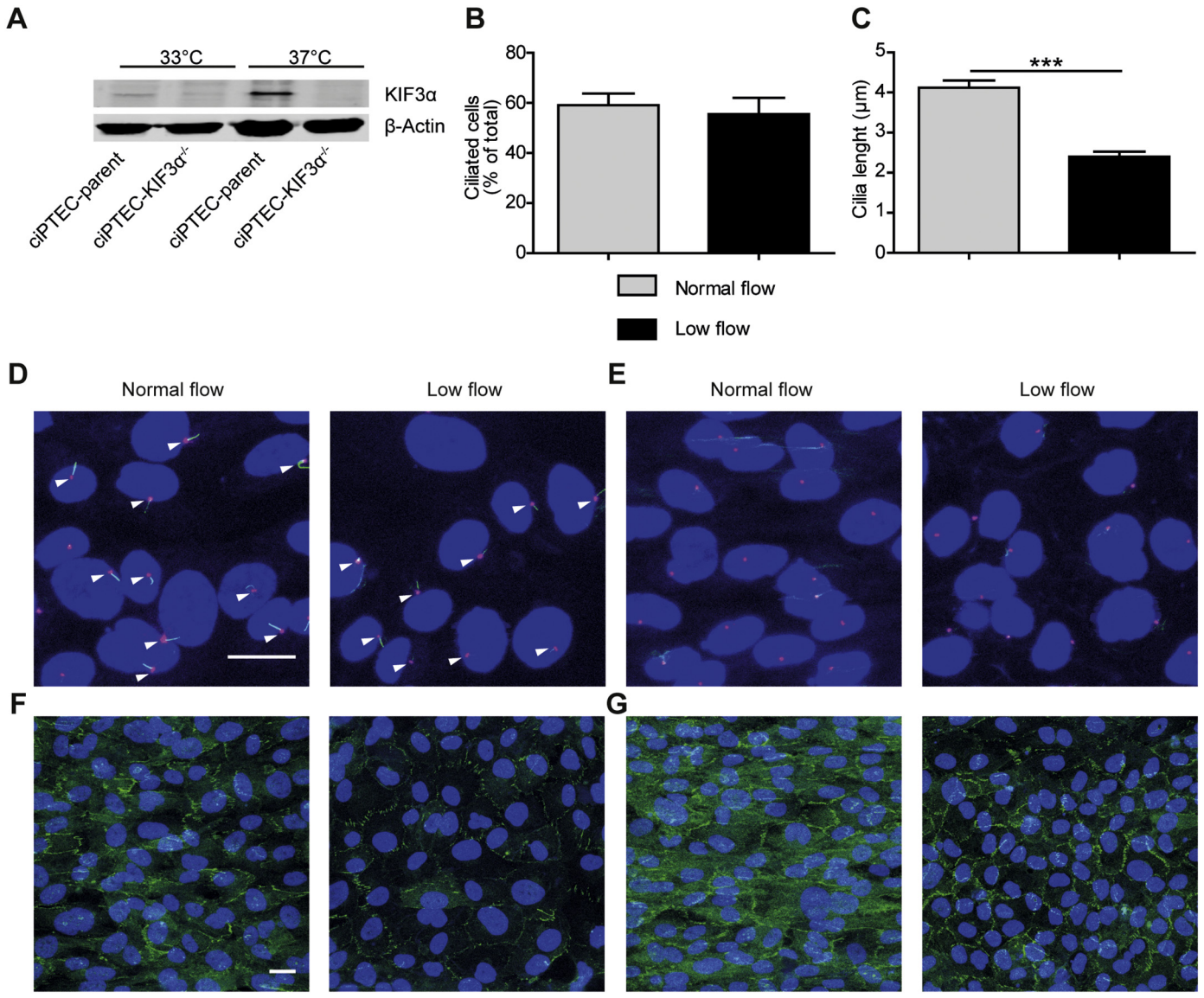

Fig. 3. Characteristics of proximal tubule epithelial cells (PTECs) in ciPTEC-parent and ciPTEC-KIF3α$^{-/-}$ exposed to normal and low flow. (A) Protein levels of KIF3α in ciPTEC, demonstrated by Western blotting, in proliferating ciPTEC at 33 °C and matured ciPTEC at 37 °C. Representative image of Western blot of one of three experiments performed, β-actin was used as loading control. (B) Number of ciliated cells and (C) cilia length in ciPTEC-parent. (D) Expression of acetylated-tubulin (green), a component of primary cilia; pericentrin (magenta), a centrosome marker; and nuclei (DAPI, blue) in ciPTEC-parent and (E) ciPTEC-KIF3α$^{-/-}$. Primary cilia are annotated with white arrows. (F) Staining of tight junction protein zonula occludens 1 (ZO-1, green) and nuclei (blue) in ciPTEC-parent and (G) ciPTEC-KIF3α$^{-/-}$. Scale bar represents 20 µm in all images, images were scaled accordingly. Student's *t*-test normal flow *vs.* low flow, ***$p < .001$. (For interpretation of the references to color in this figure legend, the reader is referred to the web version of this article.)

upregulated under normal flow as compared to low flow, whereas expression of megalin, cubilin and other drug transporters were independent of flow rate. Next, albumin uptake and efflux activities of MRP2/4 and P-gp were assessed in ciPTEC-parent, cultured under normal or low flow (Fig. 2A). Cubilin- and megalin-mediated albumin uptake was determined using albumin-FITC (Fig. 2A), which was decreased 0.65 ± 0.04-fold upon co-incubation with BSA (10 mg/mL) under normal flow (Fig. 2B). When ciPTEC-parent were cultured under normal flow, albumin uptake was increased in ($p = .04$) as compared to low flow (Fig. 2B), which was abolished upon co-incubation with BSA ($p = .03$) (Fig. 2B).

MRP2/4 activity was measured using GS-MF, which is a typical substrate for both transporters and a fluorescent metabolite of the cell membrane permeable CMFDA [25]. Accumulation of GS-MF was observed in all conditions evaluated (Fig. 2A) and was increased upon exposure to a combination of inhibitors PSC833 (5 µM), MK571 (10 µM) and KO143 (10 µM), demonstrating inhibition of GS-MF efflux (Fig. 2C). This resulted in a 2.9 ± 0.3-fold and 2.1 ± 0.6-fold increased accumulation of GS-MF compared to vehicle in normal and low flow, respectively. A trend towards increased efflux of GS-MF was visible in normal flow compared to low flow (Fig. 2C) but was, however, not found to be significantly different in vehicle ($p = .06$) or upon inhibition ($p = .07$).

P-gp activity was determined using a similar method based on calcein-AM, which can freely diffuse in the cell and is a substrate for P-gp, but can also be metabolized into calcein, a fluorescent substrate for MRP2/4 [25]. In all conditions tested, intracellular accumulation of calcein was observed (Fig. 2A). Accumulation of calcein was increased by 3.8 ± 0.4-fold and 2.9 ± 0.7-fold upon co-incubation with CsA (30 µM), a known P-gp inhibitor [27], compared to vehicle in normal and low flow, respectively (Fig. 2D). Likewise, a 2.9 ± 0.3-fold and 2.6 ± 0.5-fold increased accumulation of calcein was observed upon

Table 2
Gene expression levels of drug transporters, endocytosis receptors, tight junction proteins and oxidative status markers in ciPTEC-KIF3α$^{-/-}$.

Gene	Ct values		$2^{-\Delta\Delta Ct}$	
	Normal flow	Low flow	Normal flow	Low flow
GAPDH	19.1 ± 0.2	19.1 ± 0.1		
HPRT1	26.1 ± 0.2	25.9 ± 0.2	1.0 ± 0.1	0.9 ± 0.0
ABCB1	28.2 ± 0.1	28.2 ± 0.2	1.0 ± 0.1	1.0 ± 0.2
ABCC2	33.8 ± 0.1	34.4 ± 0.1	1.0 ± 0.1	0.7 ± 0.1*
ABBC4	25.7 ± 0.2	25.7 ± 0.3	1.0 ± 0.1	1.0 ± 0.1
SLC22A2	36.5 ± 0.1	35.9 ± 0.3	1.0 ± 0.1	1.5 ± 0.1
SLC47A1	31.6 ± 0.9	31.8 ± 0.9	1.4 ± 0.8	1.1 ± 0.6
SCL47A2	34.2 ± 1.2	33.6 ± 1.1	1.9 ± 1.4	2.2 ± 1.4
LRP2	39.2 ± 0.1	39.1 ± 0.0	1.0 ± 0.1	1.1 ± 0.2
CBN	32.3 ± 0.2	32.0 ± 0.3	1.0 ± 0.1	1.2 ± 0.1
CLDN2	27.9 ± 0.4	27.5 ± 0.3	1.1 ± 0.3	1.3 ± 0.1
HMOX1	25.2 ± 0.5	25.2 ± 0.2	1.1 ± 0.4	1.0 ± 0.1
HIF1A	20.3 ± 0.2	20.5 ± 0.3	1.0 ± 0.2	0.9 ± 0.3

Levels of mRNA of drug transporters (*ABCB1, ABCC2, ABCC4, SLC22A2, SLC47A1, SLC47A2*), albumin endocytosis receptors (*LRP2, CBN*), a tight junction component (*CLDN2*) and oxidative status markers (*HMOX1, HIF1A*). Student's *t*-test normal flow *vs.* low flow, *$p < .05$.

exposure to PSC833 (5 μM), a model inhibitor of P-gp, compared to vehicle in normal and low flow, respectively (Fig. 2D). Calcein-AM efflux was significantly enhanced in normal flow compared to low flow in vehicle ($p = .002$) and upon co-incubation with PSC833 ($p = .01$), indicating that P-gp activity was enhanced under normal flow in ciPTEC-parent (Fig. 2D). However, this increased efflux was not significant upon exposure to CsA ($p = .18$).

3.2. Knock-out of primary cilium kinesin-II motor complex KIF3α

Long-term effects of primary cilium-mediated response on tubular functional parameters have never been studied in detail. We, therefore, established a primary cilium knock-out cell line by deletion of KIF3α in ciPTEC *via* CRISPR-Cas9 genome editing. KIF3α is a component of the kinesin-II motor complex, responsible for transport along the primary cilium, and has been shown to effectively knock-out the primary cilium *in vitro* and *in vivo* [20,23,28,29].

Like ciPTEC-parent, clear tubular epithelial monolayers were formed by ciPTEC-KIF3α$^{-/-}$ under normal and low flow conditions, as demonstrated by F-actin staining (Video S1). Successful knock-out of the primary cilium in ciPTEC was confirmed by protein expression levels (Fig. 3A). In ciPTEC-parent, primary cilia were clearly visible by staining of co-localized pericentrin and acetylated-tubulin, and the number of ciliated cells was similar when cells were cultured under normal (59 ± 5%) or low (56 ± 6%) flow (Fig. 3B, D). Interestingly, the length of primary cilia under normal flow (4.1 ± 0.2 μm) increased compared to low flow (2.4 ± 0.1 μm) in ciPTEC-parent (Fig. 3C). Upon knock-out of KIF3α, primary cilia were absent (Fig. 3E), further confirming our knock-out cell line. In both cell lines, ZO-1 was found to be located more pronounced towards the cytosol upon culturing under normal flow, while localization was more at lateral membranes when cultured under low flow (Fig. 3F, G).

Ca^{2+} ions are key in cell signaling and their influx is mainly mediated through the primary cilium [30,31]. Consequently, cytosolic levels of Ca^{2+} were measured in ciPTEC-parent and ciPTEC-KIF3α$^{-/-}$. Intracellular Ca^{2+} levels were similar in both cell lines when cultured under normal and low flow ($p = .99$ and $p = .72$, respectively), demonstrating that levels of cytosolic Ca^{2+} were not affected by primary cilium knock-out (Fig. S1A). Immediate flow *in situ* did not result in considerable increased levels of cytosolic Ca^{2+} in both cell lines over time (Fig. S1B).

3.3. Albumin uptake and transport activity of MRP2/4 and P-gp are not affected in a primary cilium knock-out model

Gene expression levels of drug transporters (*ABCB1*, *ABCC2*, *SLC22A2*, *SLC47A1*, *SLC47A2*), *LRP2* and *CBN* in both flow conditions were similar in ciPTEC-KIF3α$^{-/-}$, although a significant up-regulation of *ABCC2* compared to low flow was observed (Table 2). Next, we studied whether the increased albumin uptake and P-gp activity in normal flow could be explained by a primary cilium-mediated response towards FSS. Therefore, cubilin- and megalin-mediated albumin uptake and activities of the efflux transporters MRP2/4 and P-gp were measured in ciPTEC-KIF3α$^{-/-}$ when cultured under normal and low flow (Fig. 4A).

With normal flow, albumin-FITC uptake (0.74 ± 0.04-fold) was decreased upon co-incubation with BSA (Fig. 4B). In line with ciPTEC-parent, a significantly increased albumin-FITC uptake was observed in control ($p = .03$) in normal flow compared to low flow (Fig. 4B), but not upon co-incubation with BSA ($p = .32$).

MRP2/4 activity was inhibited upon exposure to PSC833, MK571 and KO143, as indicated by a 3.0 ± 0.3-fold and 2.4 ± 0.6-fold increased GS-MF accumulation compared to vehicle in normal and low flow, respectively (Fig. 4C). Similar to ciPTEC-parent, increased efflux of GS-MF was visible in normal flow compared to low flow (Fig. 4C), but was not significantly different in vehicle ($p = .11$) or upon inhibition ($p = .44$).

Accumulation of calcein was increased by 3.5 ± 0.3-fold and 3.4 ± 0.4-fold compared to vehicle in normal flow after incubation with CsA or PSC833, respectively (Fig. 4D). Furthermore, under low flow, retention of calcein was increased by 2.8 ± 1.0-fold and 2.2 ± 0.7-fold compared to vehicle after incubation with CsA or PSC833, respectively (Fig. 4D). Statistical differences between normal and low flow in vehicle ($p = .09$) or upon co-incubation with CsA ($p = .45$) or PSC833 ($p = .82$) were not found.

3.4. FSS-induced changes in PTEC cell morphology

Expression of tight junction proteins, *HMOX1* and *HIF1A* have previously been shown to increase upon exposure to FSS [2,32–34]. Gene expression levels of *CLDN2*, as marker for intercellular tight junction, were comparable in both flow conditions, as well as expression levels of oxidative stress marker *HMOX1* and hypoxia marker *HIF1A* in both ciPTEC-parent (Table 1) and ciPTEC-KIF3α$^{-/-}$ (Table 2).

Exposure to flow has been associated with changes in cell morphology and cell elongation corresponding to flow direction in 3D kidney models [1,2,35]. Cell surface area, aspect ratio and circularity were measured in single-cell masks of calcein staining in ciPTEC-parent and ciPTEC-KIF3α$^{-/-}$ (Fig. 5A, B). Different cell densities were observed in the flow conditions and cell lines (Fig. 5A, B). Cell surface area decreased when culturing under normal flow in both ciPTEC-parent and ciPTEC-KIF3α$^{-/-}$ (Fig. 5C, F). In addition, cell elongation aligning with the axis flow direction was observed upon exposure to normal flow, correlating with a higher aspect ratio in both cell lines (Fig. 5D, G) and decreased circularity in ciPTEC-parent (Fig. 5E).

3.5. Cytotoxic response to cyclosporine A is not related to enhanced P-gp activity under normal flow

CsA is a known nephrotoxicant and reported to induce damage to the endoplasmic reticulum (ER) and mitochondria, and increases oxidative stress in PTECs [36,37]. P-gp activity was decreased upon exposure to CsA as demonstrated by the increased accumulation of calcein in both ciPTEC-parent (Fig. 2D) and ciPTEC-KIF3α$^{-/-}$ (Fig. 4D). In addition, P-gp activity was enhanced in ciPTEC-parent cultured under normal flow in vehicle, although no difference in activity was found after co-incubation with CsA (Fig. 2D). Since CsA-induced cytotoxicity

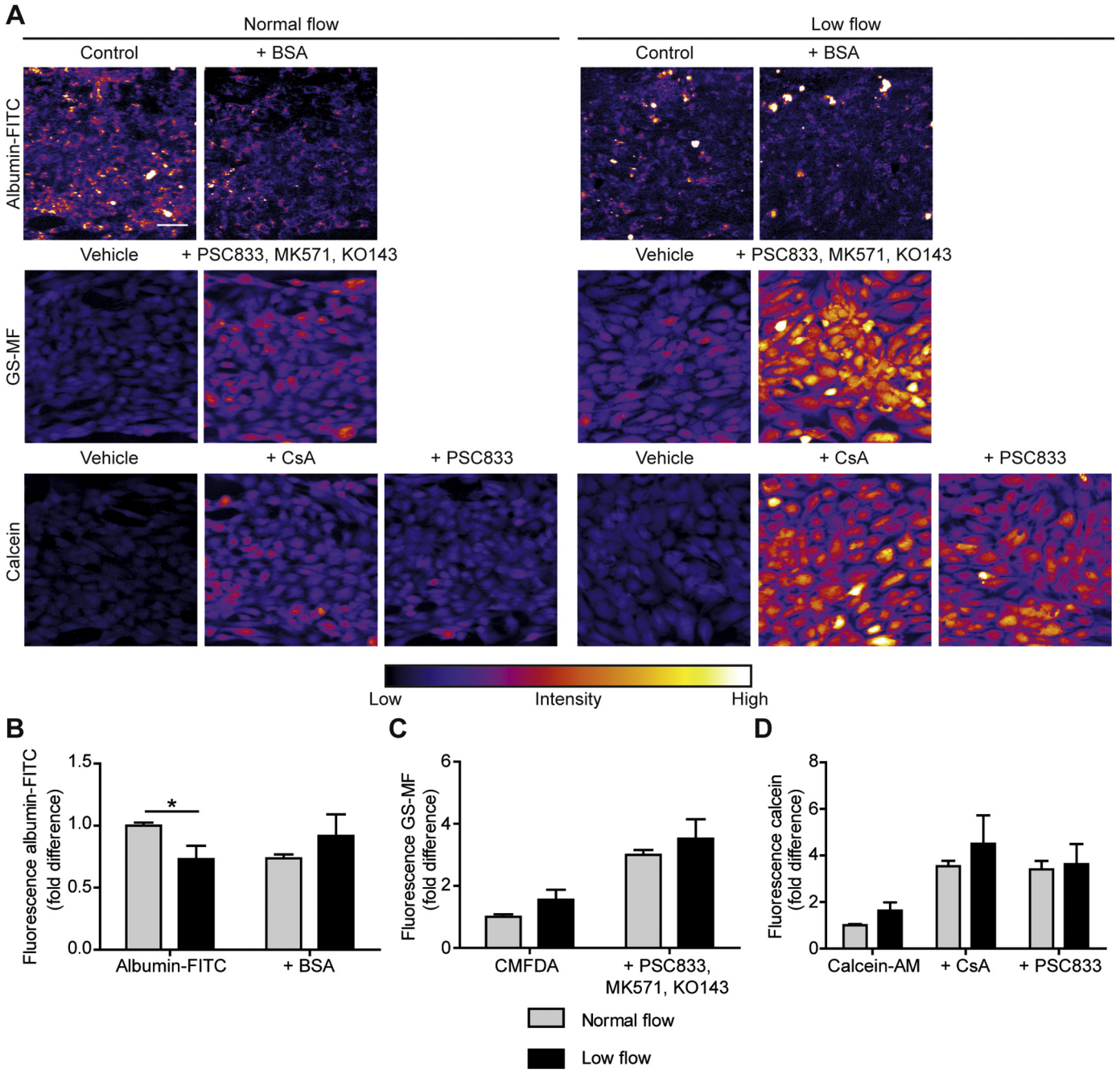

Fig. 4. Albumin uptake and efflux activity of P-glycoprotein (P-gp) and multidrug resistance-associated proteins 2 and 4 (MRP2/4) in ciPTEC-KIF3α$^{-/-}$, as cilium knock-out model, cultured under normal and low flow in the OrganoPlate. (A) Representative images of intracellular accumulation of albumin-fluorescein isothiocyanate conjugate (albumin-FITC), glutathione-methylfluorescein (GS-MF) and calcein. Albumin-FITC uptake was observed in all conditions, but decreased upon exposure with bovine serum albumin (BSA, 10 mg/mL) in normal FSS. In all conditions, accumulation of GS-MF was demonstrated, which was increased upon incubation with a mixture of inhibitors PSC833 (5 μM), MK571 (10 μM), KO143 (10 μM). Calcein accumulation was visible in all conditions and increased upon exposure to cyclosporine A (CsA, 30 μM) or PSC833 (5 μM). To enhance contrast for presentation, display ranges of albumin-FITC, GS-MF and calcein images were set to 0 to 600, 0 to 900 and 0 to 1800, respectively. Gray scale values were converted to look-up table (LUT) color fire. Scale bar represents 50 μm, scale in all images are equal. Fluorescent signal was quantified, corrected for nuclei count, using Hoechst33342 (20 μg/mL), and normalized to fluorescence measured in vehicle in normal flow for (B) albumin-FITC, (C) GS-MF and (D) calcein. Student's *t*-test normal flow *vs.* low flow, $*p < .05$.

could have been more severe in low flow because of a lower P-gp activity, we investigated the cytotoxic response to CsA (30 μM) after 24 h in both flow conditions and cell lines (Fig. 6). In ciPTEC-parent (Fig. 6A), cell viability was reduced upon CsA exposure at normal (94 ± 1%) and low flow (95 ± 1%). Even though P-gp activity was found to be decreased in low flow in ciPTEC-parent, this did not result in an increased CsA-induced cytotoxicity (Fig. 6A). Interestingly, ciPTEC-KIF3α$^{-/-}$ was more sensitive to CsA-induced cytotoxicity compared to ciPTEC-parent, regardless of flow (Fig. 6B), resulting in decreased cell viability when exposed to normal or low flow (both 71 ± 4%). This indicates that a primary cilium-associated mechanism, other than triggered by flow, is involved in a more sensitive phenotype of ciPTEC-KIF3α$^{-/-}$.

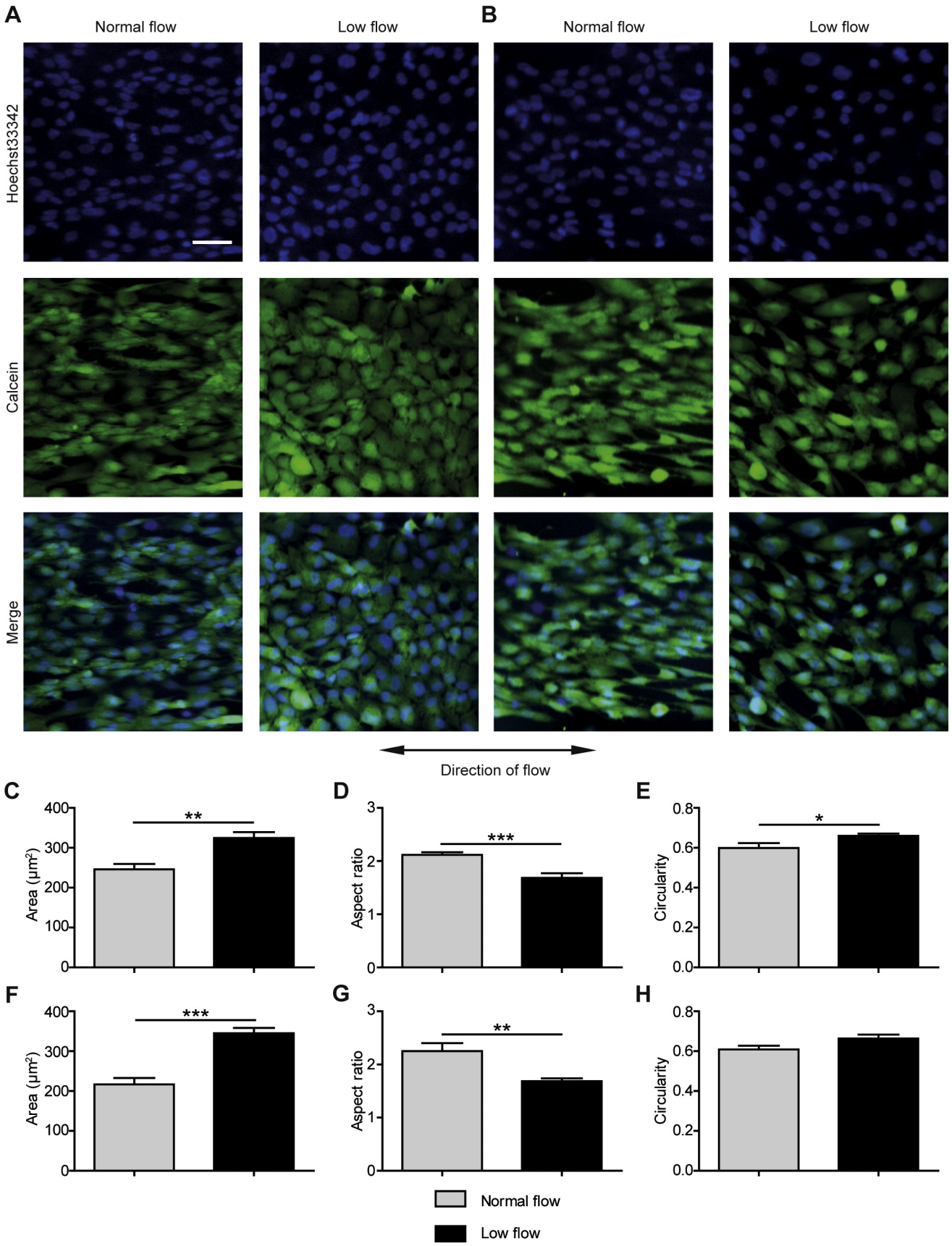

Fig. 5. Live cell imaging demonstrated changes in cell morphology of ciPTEC-parent and ciPTEC-KIF3α$^{-/-}$ when exposed to fluid shear stress (FSS). (A) In ciPTEC-parent and (B) ciPTEC-KIF3α$^{-/-}$ cytoplasm and nuclei were stained using calcein-AM (2 µM) and Hoechst33342 (20 µg/mL), respectively. Scale bar represents 50 µm. Single-cell analysis of cell area, aspect ratio and circularity in (C-E) ciPTEC-parent and (F-H) ciPTEC-KIF3α$^{-/-}$. Student's *t*-test normal flow *vs.* low flow, $*p < .05$, $**p < .01$, $***p < .001$.

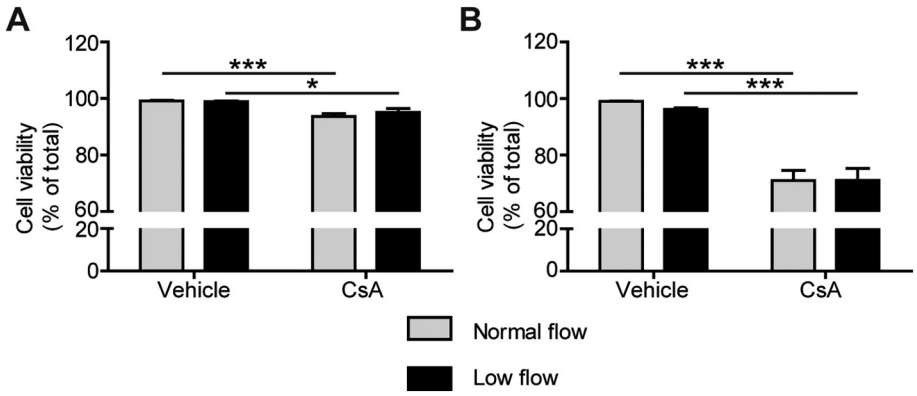

Fig. 6. Cell viability after exposure (24 h) to vehicle or cyclosporine A (CsA, 30 μM). Upon exposure, cell viability in (A) ciPTEC-parent and (B) ciPTEC-KIF3α$^{-/-}$ was determined as sum of necrotic cells, stained with propidium iodide (1 μg/mL), and apoptotic cells, stained with YO-PRO-1 (2 μM), divided by total number nuclei, stained with Hoechst33342 (20 μg/mL). Two-way ANOVA, followed by Tukey's *post hoc* analysis, vehicle *vs.* CsA treatment in corresponding flow condition, *$p < .05$, ***$p < .001$.

4. Discussion

Our study demonstrates for the first time that FSS-induced increased albumin uptake, drug efflux, and elongated phenotype in PTECs are independent of primary cilia. We observed significantly increased albumin uptake, P-gp activity and phenotypical morphological changes when culturing immortalized PTECs under a physiologically relevant pulsatile FSS in the OrganoPlate. We established a cell line devoid of a primary cilium by depleting KIF3α gene, of which *in vivo* mutants are associated with the formation of cysts, a severe renal disorder [20,38].

The increased P-gp activity and albumin uptake in renal cells when cultured under FSS as observed here, are in line with earlier studies [1,2,15,16]. A primary cilium-mediated mechanosensitive response was attributed to explain these findings, as the number of ciliated cells and length of cilia were increased under flow [2,19]. Deciliation of opossum kidney (OK) cells using ammonium sulfate diminished the flow-induced increase in albumin uptake at short-term (1 − 3 h) exposure to flow [15,16]. A similar approach diminished flow-induced increased organic cation transport in Madine Darby Canine Kidney II (MDCKII) cells double-transfected with OCT2 and MATE1 [17]. In contrast, our results argue for a minor role of the primary cilium in regulating drug transporter expression as the knockout cells behaved similarly to ciPTEC-parent when exposed to FSS. This might be explained by the method of deciliation and the cell model used, as MDCK II represent renal collecting duct cells rather than PTECs [39]. Previous studies only showed short-term chemical deciliation for up to 24 h [15,17], whereas we knocked-out the primary cilium completely from PTECs through gene editing. An explanation for our findings could be the apical expression of microvilli in addition to primary cilia in our immortalized cell model [40]. Microvilli length and density increased in 3D proximal tubules cultured under flow, demonstrating that microvilli also respond to flow in PTECs [1]. Although deletion of microvilli can be performed *via* genetic knock-out of ezrin that connects the actin cytoskeleton to the plasma membrane, this will also affect the bending of the primary cilium and the glycocalyx [18,41]. Further, primary cilia increased in length upon exposure to a physiological FSS, demonstrating that a FSS-induced response triggered the primary cilium in line with findings in osteocytes, where longer primary cilia increased mechanosensitivity [42]. However, ciPTEC-KIF3α$^{-/-}$ showed a similar response to FSS as determined by enhanced albumin uptake, P-gp activity and cell elongation, suggesting these flow effects are independent of primary cilia.

Although primary cilia seem to be key in Ca^{2+} signaling, and the influx of extracellular Ca^{2+} was long thought to be mediated through polycystin-1 and -2 upon FSS-induced mechanosensation in kidney cells [30,31], more recent data contradict this model [43]. In line with this, we did not observe any differences in levels of cytosolic Ca^{2+} in primary cilium knock-out cells. Furthermore, FSS affected levels of cytosolic Ca^{2+} in both cell lines and thus regardless of the presence of primary cilia. On the other hand, microvilli have an important mechanosensory function modulating transport and cytoskeletal reorganization in PTECs and not *via* primary cilia-mediated signaling [13,44,45]. This aligns with our observations on FSS-induced increase in albumin uptake, P-gp efflux and cell elongation, regardless of the presence of primary cilia in our cell model.

In most proximal tubule-on-a-chip devices, PTECs were cultured under flow in a flat monolayer and a pump was required to induce flow [2,15,16]. FSS in a tubular structure is different compared to that in a flat monolayer on the bottom [18]. Tubule-like structures were demonstrated in all conditions tested and tubular stretch was incorporated in this proximal tubule-on-a-chip. Here, epithelial tubules were cultured under an intermittent pulsatile flow, comparable to *in vivo* conditions, and subsequently exposed to different peak FSS. A bi-directional gravity-induced flow was generated by leveling of the culture plate on an interval rocker platform, circumventing the use of pumps as applied in most other microfluidics studies.

Furthermore, proximal tubule-on-a-chip devices have great potential for implementation in pre-clinical drug safety assessment to predict DIKI because of closer resemblance of *in vivo* environment in PTEC [1–3,35]. CsA, a known nephrotoxicant [36,37], did not increase cytotoxicity in low flow as result of a decreased P-gp activity compared to normal flow. Our primary cilium knock-out model, however, was more sensitive to CsA-induced cytotoxicity compared to ciPTEC-parent, regardless of flow. Increased sensitivity towards cisplatin-induced apoptosis has been described previously in a KIF3α knock-out model in human kidney-2 (HK-2) cells [29]. This cisplatin-induced increased apoptosis was suggested to be caused by ERK-mediated disruption of primary cilia [29], and could explain the increased sensitivity towards CsA-induced cytotoxicity as observed in our primary cilium knock-out model.

5. Conclusion

We demonstrated that FSS induced increased albumin uptake and P-gp activity, and improves cell morphology in a proximal tubule-on-a-chip. These effects were not attributed to a mechanosensitive mechanism related to primary cilium function, but likely to microvilli present at the apical membrane.

Supplementary data to this article can be found online at https://doi.org/10.1016/j.bbagen.2019.129433.

Author contributions

Jelle Vriend: Conceptualization, Methodology, Investigation, Formal Analysis, Writing - Original Draft. Janny Peters and Tom Nieskens: Conceptualization, Methodology, Investigation, Writing - Original Draft. Renata Škovroňová and Nina Blaimschein: Investigation, Writing - Reviewing and Editing. Miriam Schmidts: Methodology, Resources, Writing - Reviewing and Editing. Ronald Roepman: Conceptualization, Methodology, Writing - Reviewing and Editing. Tom

Schirris and Frans Russel: Conceptualization, Methodology, Writing - Original Draft. Rosalinde Masereeuw: Conceptualization, Methodology, Formal Analysis, Writing - Original Draft. Martijn Wilmer: Conceptualization, Methodology, Writing - Original Draft, Supervision, Funding Acquisition.

Declaration of Competing Interest

Martijn Wilmer and Frans Russel are co-inventors on patent EP2010/066792 "Novel conditionally immortalized human proximal tubule cell line expressing functional influx and efflux transporters" assigned to Radboud University Medical Center and commercialized through Cell4Pharma.com.

Acknowledgements

This project received financial support under the Crack-it challenge 15 (Nephrotube) project no. 37497-25920, an initiative of the National Centre for the Replacement, Refinement and Reduction of Animals in Research (NC3Rs). The authors thank Henriette L. Lanz and Bjorn de Wagenaar (Mimetas, Leiden, The Netherlands) for their advice regarding fluid shear stress in the OrganoPlate, and Alexander H. van Asbeck (Department of Biochemistry, Radboud University Medical Center) for assistance in CRISPR-Cas9 genome editing. Miriam Schmidts acknowledges funding from the Radboud University Medical Center (Hypatia tenure track grant) and the European Research Council (ERC starting grant TREATCilia, grant agreement no. 716344).

References

[1] K.A. Homan, D.B. Kolesky, M.A. Skylar-Scott, J. Herrmann, H. Obuobi, A. Moisan, J.A. Lewis, Bioprinting of 3D convoluted renal proximal tubules on perfusable chips, Sci. Rep. 6 (2016) 34845, , https://doi.org/10.1038/srep34845.

[2] K.J. Jang, A.P. Mehr, G.A. Hamilton, L.A. McPartlin, S. Chung, K.Y. Suh, D.E. Ingber, Human kidney proximal tubule-on-a-chip for drug transport and nephrotoxicity assessment, Integr. Biol. 5 (2013) 1119–1129, https://doi.org/10.1039/c3ib40049b.

[3] E.J. Weber, A. Chapron, B.D. Chapron, J.L. Voellinger, K.A. Lidberg, C.K. Yeung, Z. Wang, Y. Yamaura, D.W. Hailey, T. Neumann, D.D. Shen, K.E. Thummel, K.A. Muczynski, J. Himmelfarb, E.J. Kelly, Development of a microphysiological model of human kidney proximal tubule function, Kidney Int. 90 (2016) 627–637, https://doi.org/10.1016/j.kint.2016.06.011.

[4] S. Peel, A.M. Corrigan, B. Ehrhardt, K.J. Jang, P. Caetano-Pinto, M. Boeckeler, J.E. Rubins, K. Kodella, D.B. Petropolis, J. Ronxhi, G. Kulkarni, A.J. Foster, D. Williams, G.A. Hamilton, L. Ewart, Introducing an automated high content confocal imaging approach for Organs-on-Chips, Lab Chip 19 (2019) 410–421, https://doi.org/10.1039/c8lc00829a.

[5] N.Y.C. Lin, K.A. Homan, S.S. Robinson, D.B. Kolesky, N. Duarte, A. Moisan, J.A. Lewis, Renal reabsorption in 3D vascularized proximal tubule models, Proc. Natl. Acad. Sci. U. S. A. (2019), https://doi.org/10.1073/pnas.1815208116.

[6] J.Y. Soo, J. Jansen, R. Masereeuw, M.H. Little, Advances in predictive in vitro models of drug-induced nephrotoxicity, Nat. Rev. Nephrol. 14 (2018) 378–393, https://doi.org/10.1038/s41581-018-0003-9.

[7] A. Ivanyuk, F. Livio, J. Biollaz, T. Buclin, Renal drug transporters and drug interactions, Clin. Pharmacokinet. 56 (2017) 825–892, https://doi.org/10.1007/s40262-017-0506-8.

[8] M.L. Eshbach, O.A. Weisz, Receptor-mediated endocytosis in the proximal tubule, Annu. Rev. Physiol. 79 (2017) 425–448, https://doi.org/10.1146/annurev-physiol-022516-034234.

[9] J. Vriend, T.T.G. Nieskens, M.K. Vormann, B.T. van den Berge, A. van den Heuvel, F.G.M. Russel, L. Suter-Dick, H.L. Lanz, P. Vulto, R. Masereeuw, M.J. Wilmer, Screening of drug-transporter interactions in a 3D microfluidic renal proximal tubule on a chip, AAPS J. 20 (2018) 87, https://doi.org/10.1208/s12248-018-0247-0.

[10] M.K. Vormann, L. Gijzen, S. Hutter, L. Boot, A. Nicolas, A. van den Heuvel, J. Vriend, C.P. Ng, T.T.G. Nieskens, V. van Duinen, B. de Wagenaar, R. Masereeuw, L. Suter-Dick, S.J. Trietsch, M. Wilmer, J. Joore, P. Vulto, H.L. Lanz, Nephrotoxicity and kidney transport assessment on 3D perfused proximal tubules, AAPS J. 20 (2018) 90, https://doi.org/10.1208/s12248-018-0248-z.

[11] J.R. Levick, L.H. Smaje, An analysis of the permeability of a fenestra, Microvasc. Res. 33 (1987) 233–256.

[12] K.J. Jang, H.S. Cho, D.H. Kang, W.G. Bae, T.H. Kwon, K.Y. Suh, Fluid-shear-stress-induced translocation of aquaporin-2 and reorganization of actin cytoskeleton in renal tubular epithelial cells, Integr. Biol. 3 (2011) 134–141, https://doi.org/10.1039/c0ib00018c.

[13] Y. Duan, N. Gotoh, Q. Yan, Z. Du, A.M. Weinstein, T. Wang, S. Weinbaum, Shear-induced reorganization of renal proximal tubule cell actin cytoskeleton and apical junctional complexes, Proc. Natl. Acad. Sci. U. S. A. 105 (2008) 11418–11423, https://doi.org/10.1073/pnas.0804954105.

[14] M. Essig, F. Terzi, M. Burtin, G. Friedlander, Mechanical strains induced by tubular flow affect the phenotype of proximal tubular cells, Am. J. Physiol. Ren. Physiol. 281 (2001) F751–F762, https://doi.org/10.1152/ajprenal.2001.281.4.F751.

[15] V. Raghavan, Y. Rbaibi, N.M. Pastor-Soler, M.D. Carattino, O.A. Weisz, Shear stress-dependent regulation of apical endocytosis in renal proximal tubule cells mediated by primary cilia, Proc. Natl. Acad. Sci. U. S. A. 111 (2014) 8506–8511, https://doi.org/10.1073/pnas.1402195111.

[16] S. Bhattacharyya, F.G. Jean-Alphonse, V. Raghavan, J.C. McGarvey, Y. Rbaibi, J.P. Vilardaga, M.D. Carattino, O.A. Weisz, Cdc42 activation couples fluid shear stress to apical endocytosis in proximal tubule cells, Phys. Rep. 5 (2017), https://doi.org/10.14814/phy2.13460.

[17] A. Jayagopal, P. Brakeman, P. Soler, N. Ferrell, W. Fissell, D.L. Kroetz, S. Roy, Apical shear stress enhanced organic cation transport in hOCT2/hMATE1 transfected MDCK cells involves ciliary sensing, J. Pharmacol. Exp. Ther. (2019), https://doi.org/10.1124/jpet.118.255026.

[18] V. Raghavan, O.A. Weisz, Discerning the role of mechanosensors in regulating proximal tubule function, Am. J. Physiol. Ren. Physiol. 310 (2016) F1–F5, https://doi.org/10.1152/ajprenal.00373.2015.

[19] K.A. Homan, N. Gupta, K.T. Kroll, D.B. Kolesky, M. Skylar-Scott, T. Miyoshi, D. Mau, M.T. Valerius, T. Ferrante, J.V. Bonventre, J.A. Lewis, R. Morizane, Flow-enhanced vascularization and maturation of kidney organoids in vitro, Nat. Methods 16 (2019) 255–262, https://doi.org/10.1038/s41592-019-0325-y.

[20] J.R. Marszalek, P. Ruiz-Lozano, E. Roberts, K.R. Chien, L.S. Goldstein, Situs inversus and embryonic ciliary morphogenesis defects in mouse mutants lacking the KIF3A subunit of kinesin-II, Proc. Natl. Acad. Sci. U. S. A. 96 (1999) 5043–5048.

[21] M.J. Wilmer, M.A. Saleem, R. Masereeuw, L. Ni, T.J. van der Velden, F.G. Russel, P.W. Mathieson, L.A. Monnens, L.P. van den Heuvel, E.N. Levtchenko, Novel conditionally immortalized human proximal tubule cell line expressing functional influx and efflux transporters, Cell Tissue Res. 339 (2010) 449–457, https://doi.org/10.1007/s00441-009-0882-y.

[22] Z. Cai, J. Xin, D.M. Pollock, J.S. Pollock, Shear stress-mediated no production in inner medullary collecting duct cells, Am. J. Physiol. Ren. Physiol. 279 (2000) F270–F274, https://doi.org/10.1152/ajprenal.2000.279.2.F270.

[23] L.B. Hoang-Minh, L.P. Deleyrolle, N.S. Nakamura, A.K. Parker, R.T. Martuscello, B.A. Reynolds, M.R. Sarkisian, PCM1 depletion inhibits glioblastoma cell ciliogenesis and increases cell death and sensitivity to temozolomide, Transl. Oncol. 9 (2016) 392–402, https://doi.org/10.1016/j.tranon.2016.08.006.

[24] F.A. Ran, P.D. Hsu, J. Wright, V. Agarwala, D.A. Scott, F. Zhang, Genome engineering using the CRISPR-Cas9 system, Nat. Protoc. 8 (2013) 2281–2308, https://doi.org/10.1038/nprot.2013.143.

[25] P. Caetano-Pinto, M.J. Janssen, L. Gijzen, L. Verscheijden, M.J. Wilmer, R. Masereeuw, Fluorescence-based transport assays revisited in a human renal proximal tubule cell line, Mol. Pharm. 13 (2016) 933–944, https://doi.org/10.1021/acs.molpharmaceut.5b00821.

[26] J. Schindelin, I. Arganda-Carreras, E. Frise, V. Kaynig, M. Longair, T. Pietzsch, S. Preibisch, C. Rueden, S. Saalfeld, B. Schmid, J.Y. Tinevez, D.J. White, V. Hartenstein, K. Eliceiri, P. Tomancak, A. Cardona, Fiji: an open-source platform for biological-image analysis, Nat. Methods 9 (2012) 676–682, https://doi.org/10.1038/nmeth.2019.

[27] J.W. Polli, S.A. Wring, J.E. Humphreys, L. Huang, J.B. Morgan, L.O. Webster, C.S. Serabjit-Singh, Rational use of in vitro p-glycoprotein assays in drug discovery, J. Pharmacol. Exp. Ther. 299 (2001) 620–628.

[28] N. Arrighi, K. Lypovetska, C. Moratal, S. Giorgetti-Peraldi, C.A. Dechesne, C. Dani, P. Peraldi, The primary cilium is necessary for the differentiation and the maintenance of human adipose progenitors into myofibroblasts, Sci. Rep. 7 (2017) 15248, , https://doi.org/10.1038/s41598-017-15649-2.

[29] S. Wang, Q. Wei, G. Dong, Z. Dong, ERK-mediated suppression of cilia in cisplatin-induced tubular cell apoptosis and acute kidney injury, Biochim. Biophys. Acta 1832 (2013) 1582–1590, https://doi.org/10.1016/j.bbadis.2013.05.023.

[30] M. Delling, P.G. DeCaen, J.F. Doerner, S. Febvay, D.E. Clapham, Primary cilia are specialized calcium signalling organelles, Nature 504 (2013) 311–314, https://doi.org/10.1038/nature12833.

[31] S.M. Nauli, F.J. Alenghat, Y. Luo, E. Williams, P. Vassilev, X. Li, A.E. Elia, W. Lu, E.M. Brown, S.J. Quinn, D.E. Ingber, J. Zhou, Polycystins 1 and 2 mediate mechanosensation in the primary cilium of kidney cells, Nat. Genet. 33 (2003) 129–137, https://doi.org/10.1038/ng1076.

[32] Y. Fukuda, M. Kaishima, T. Ohnishi, K. Tohyama, I. Chisaki, Y. Nakayama, M. Ogasawara-Shimizu, Y. Kawamata, Fluid shear stress stimulates MATE2-K expression via Nrf2 pathway activation, Biochem. Biophys. Res. Commun. 484 (2017) 358–364, https://doi.org/10.1016/j.bbrc.2017.01.124.

[33] S.J. Kunnen, T.B. Malas, C. Formica, W.N. Leonhard, P.A.C.T. Hoen, D.J.M. Peters, Comparative transcriptomics of shear stress treated Pkd1(−/−) cells and pre-cystic kidneys reveals pathways involved in early polycystic kidney disease, Biomed. Pharmacother. 108 (2018) 1123–1134, https://doi.org/10.1016/j.biopha.2018.07.178.

[34] Q. Ren, M.L. Gliozzi, N.L. Rittenhouse, L.R. Edmunds, Y. Rbaibi, J.D. Locker, A.C. Poholek, M.J. Jurczak, C.J. Baty, O.A. Weisz, Shear stress and oxygen availability drive differential changes in ok proximal tubule cell metabolism and endocytosis, Traffic (2019), https://doi.org/10.1111/tra.12648.

[35] C. Sakolish, E.J. Weber, E.J. Kelly, J. Himmelfarb, R. Mouneimne, F.A. Grimm, J.S. House, T. Wade, A. Han, W.A. Chiu, I. Rusyn, Technology transfer of the microphysiological systems: a case study of the human proximal tubule tissue chip, Sci. Rep. 8 (2018) 14882, , https://doi.org/10.1038/s41598-018-33099-2.

[36] G. de Arriba, M. Calvino, S. Benito, T. Parra, Cyclosporine A-induced apoptosis in

renal tubular cells is related to oxidative damage and mitochondrial fission, Toxicol. Lett. 218 (2013) 30–38, https://doi.org/10.1016/j.toxlet.2013.01.007.
[37] P. Justo, C. Lorz, A. Sanz, J. Egido, A. Ortiz, Intracellular mechanisms of cyclosporin A-induced tubular cell apoptosis, J. Am. Soc. Nephrol. 14 (2003) 3072–3080.
[38] F. Lin, T. Hiesberger, K. Cordes, A.M. Sinclair, L.S. Goldstein, S. Somlo, P. Igarashi, Kidney-specific inactivation of the KIF3A subunit of kinesin-II inhibits renal ciliogenesis and produces polycystic kidney disease, Proc. Natl. Acad. Sci. U. S. A. 100 (2003) 5286–5291, https://doi.org/10.1073/pnas.0836980100.
[39] D.A. Herzlinger, T.G. Easton, G.K. Ojakian, The MDCK epithelial cell line expresses a cell surface antigen of the kidney distal tubule, J. Cell Biol. 93 (1982) 269–277.
[40] J. Jansen, I.E. De Napoli, M. Fedecostante, C.M. Schophuizen, N.V. Chevtchik, M.J. Wilmer, A.H. van Asbeck, H.J. Croes, J.C. Pertijs, J.F. Wetzels, L.B. Hilbrands, L.P. van den Heuvel, J.G. Hoenderop, D. Stamatialis, R. Masereeuw, Human proximal tubule epithelial cells cultured on hollow fibers: living membranes that actively transport organic cations, Sci. Rep. 5 (2015) 16702, , https://doi.org/10.1038/srep16702.
[41] V.L. Bonilha, M.E. Rayborn, I. Saotome, A.I. McClatchey, J.G. Hollyfield, Microvilli defects in retinas of ezrin knockout mice, Exp. Eye Res. 82 (2006) 720–729, https://doi.org/10.1016/j.exer.2005.09.013.
[42] M. Spasic, C.R. Jacobs, Lengthening primary cilia enhances cellular mechanosensitivity, Eur. Cell. Mater. 33 (2017) 158–168, https://doi.org/10.22203/eCM.v033a12.
[43] M. Delling, A.A. Indzhykulian, X. Liu, Y. Li, T. Xie, D.P. Corey, D.E. Clapham, Primary cilia are not calcium-responsive mechanosensors, Nature 531 (2016) 656–660, https://doi.org/10.1038/nature17426.
[44] Z. Du, S. Weinbaum, A.M. Weinstein, T. Wang, Regulation of glomerulotubular balance. III. Implication of cytosolic calcium in flow-dependent proximal tubule transport, Am. J. Physiol. Ren. Physiol. 308 (2015) F839–F847, https://doi.org/10.1152/ajprenal.00601.2014.
[45] Z. Du, Y. Duan, Q. Yan, A.M. Weinstein, S. Weinbaum, T. Wang, Mechanosensory function of microvilli of the kidney proximal tubule, Proc. Natl. Acad. Sci. U. S. A. 101 (2004) 13068–13073, https://doi.org/10.1073/pnas.0405179101.